Comparison and verification of enthalpy schemes for polythermal glaciers and ice sheets with a one-dimensional model

Heinz Blatter[a,b], Ralf Greve[a]

[a] *Institute of Low Temperature Science, Hokkaido University, Kita-19, Nishi-8, Kita-ku, Sapporo 060-0819, Japan*
[b] *Institute for Atmospheric and Climate Science, ETH Zurich, Universitätstrasse 16, CH-8092 Zurich, Switzerland*

Corresponding author: Ralf Greve (greve@lowtem.hokudai.ac.jp)

Abstract

The enthalpy method for the thermodynamics of polythermal glaciers and ice sheets is tested and verified by a one-dimensional problem (parallel-sided slab). The enthalpy method alone does not include explicitly the transition conditions at the cold-temperate transition surface (CTS) that separates the upper cold from the lower temperate layer. However, these conditions are important for correctly determining the position of the CTS. For the numerical solution of the polythermal slab problem, we consider a two-layer front-tracking scheme as well as three different one-layer schemes (conventional one-layer scheme, one-layer melting CTS scheme, one-layer freezing CTS scheme). Computed steady-state temperature and water-content profiles are verified with exact solutions, and transient solutions computed by the one-layer schemes are compared with those of the two-layer scheme, considered to be a reliable reference. While the conventional one-layer scheme (that does not include the transition conditions at the CTS) can produce correct solutions for melting conditions at the CTS, it is more reliable to enforce the transition conditions explicitly. For freezing conditions, it is imperative to enforce them because the conventional one-layer scheme cannot handle the associated discontinuities. The suggested numerical schemes are suitable for implementation in three-dimensional glacier and ice-sheet models.

Keywords:
Glacier, Ice sheet, Polythermal ice, Modeling, Enthalpy method

1. Introduction

The decrease of the ice viscosity with increasing content of liquid water in temperate ice was first confirmed and measured by Duval (1977). It is therefore desirable to simulate the water content in glaciers and ice sheets realistically, especially if the temperate ice occurs in a basal layer where shear deformation is largest. Mathematical models of polythermal ice masses were introduced and further developed by Fowler and Larson (1978), Hutter (1982), Fowler (1984) and Hutter (1993). We distinguish essentially two types of polythermal glaciers, Canadian-type polythermal glaciers, which are cold in most of the ice mass except for a temperate basal layer in the ablation zone, and Scandinavian-type glaciers, which are temperate in most parts except for a cold surface layer in the ablation zone (Fig. 1) (Blatter and Hutter, 1991).

This work attempts to verify thermodynamic schemes used in shallow ice sheet models. Therefore, we do not investigate processes which are not usually included in ice sheet models, such as possible diffusion of water in temperate ice (Hutter, 1993) and pre-melting in ice at sub-freezing temperatures (Dash et al., 2006). For verification of numerical solutions with exact solutions, we neglect the pressure dependence of the melting point and the temperature dependence of the heat conductivity and specific heat capacity. Following Aschwanden and Blatter (2005), "ice is treated as temperate if a change in heat content leads to a change in liquid water content alone, and is considered cold if a change in heat content leads to a temperature change alone." This implies that temperate ice is at the melting point and the temperatures in cold ice are below the melting point.

Polythermal schemes that solve the field equations for the cold and temperate layers separately were implemented for both types of polythermal glaciers, in one dimension for the Scandinavian-type Storglaciären, Sweden (Pettersson et al., 2007), in two dimensions for the Canadian-type Laika Glacier, Canada (Blatter and Hutter, 1991) and for

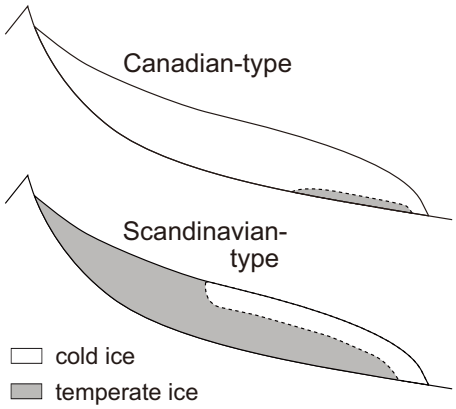

Figure 1: Schematic cross sections of Canadian- and Scandinavian-type polythermal glaciers (adapted from Aschwanden et al., 2012).

three-dimensional ice sheets, which are Canadian-type polythermal (Greve, 1997). With the assumption that water mostly accumulates along the trajectories of ice particles in the temperate layer, Aschwanden and Blatter (2005) used a trajectory model to determine the position of the cold-temperate transition surface (CTS) and the water content in the temperate part of Storglaciären. Aschwanden et al. (2012) suggested an enthalpy scheme with the idea that, with enthalpy, only one thermodynamic field variable must be computed, and the temperature and water content result from the enthalpy as diagnostic fields. The domains of cold and temperate ice are discriminated by the contour of the enthalpy of ice with no liquid water content at the melting point.

A crucial point in polythermal enthalpy schemes is their treatment of the Stefan-type energy- and mass-flux matching conditions at the CTS, which are important for determining its position (Greve, 1997). These transition conditions are not included explicitly in the formulation of the enthalpy scheme according to Aschwanden et al. (2012).

Two different cases must be distinguished. Melting conditions occur if cold ice flows across the CTS into the temperate region. At the CTS, the particles consist of ice at melting temperature without liquid water, and, after the transition, start to accumulate water due to strain heating. Thus, the boundary condition on the temperate side of the CTS is zero water content. To match the vanishing latent heat flux, the diffusive heat flux and corresponding enthalpy gradient on the cold side must also vanish.

The situation is different for freezing conditions at the CTS, where the ice flows from the temperate region into the cold region and the liquid water content of the temperate ice freezes at the CTS. The advective latent heat flux on the temperate side then changes into a diffusive heat flux on the cold side. Thus, a drop of a non-vanishing water content to zero results in a non-vanishing temperature (enthalpy) gradient in the cold layer at the CTS.

This work attempts to verify and test modified enthalpy methods, and in particular to test how the modified schemes handle the internal boundary between cold and temperate ice. For the verification, we use an exact solution which is available for steady states in a parallel-sided slab, which reduces the problem to one dimension (Greve, 1997; Greve and Blatter, 2009). In Section 2, we review the main concepts of the enthalpy method, and in Section 3, we formulate the enthalpy method for the special case of the parallel-sided slab. Section 4 deals with different one- and two-layer methods to solve this problem, the two-layer front-tracking scheme being used to provide reference solutions against which the performance of the simpler one-layer methods can be tested. Concrete numerical experiments are defined in Section 5, and results are presented and discussed in Sections 6 and 7.

2. Enthalpy formulation

In this paper we follow the formulation of Aschwanden et al. (2012) and use the notation of Greve and Blatter (2009). All physical parameters, namely the stress exponent $n = 3$ and the rate factor $A = 5.3 \times 10^{-24}\,\mathrm{s^{-1}\,Pa^{-3}}$ of Glen's flow law, the heat conductivity of ice, $\kappa = 2.1\,\mathrm{W\,m^{-1}\,K^{-1}}$, the melting point of ice, $T_\mathrm{m} = 0°\mathrm{C}$, the density

of ice, $\rho = 910\,\mathrm{kg\,m^{-3}}$, the specific heat capacity of ice, $c = 2009\,\mathrm{J\,kg^{-1}\,K^{-1}}$, and the latent heat of fusion, $L = 3.35\times10^5\,\mathrm{J\,kg^{-1}}$, are assumed to be constant for simplicity. In particular, this means that we neglect the slightly larger density of temperate ice compared to cold ice due to the ~10% larger density of liquid water.

The liquid water content (mass fraction) of temperate ice is defined by

$$W = \frac{\rho_\mathrm{w}}{\rho}\,, \tag{1}$$

where ρ_w is the partial density of liquid water in the mixture. Let $h_\mathrm{m} = c\,T_\mathrm{m}$ be the enthalpy of ice at the melting temperature with vanishing water content. For cold ice with a temperature T and temperate ice with a water content W, the enthalpy is then given by

$$h = \begin{cases} cT\,, & T < T_\mathrm{m}\,, \\ h_\mathrm{m} + LW\,, & T = T_\mathrm{m} \text{ and } 0 \le W < 1\,, \end{cases} \tag{2}$$

and the corresponding balance equation reads

$$\rho\left(\frac{\partial h}{\partial t} + \mathbf{v}\cdot\operatorname{grad} h\right) = -\nabla\cdot\mathbf{q} + \operatorname{tr}(\mathbf{t}\cdot\mathbf{D})\,, \tag{3}$$

where t is time, $\mathbf{v}$ the velocity vector, $\mathbf{q}$ the heat flux vector, $\mathbf{t}$ the Cauchy stress tensor, $\mathbf{D}$ the strain-rate tensor, the middle dot $(\cdot)$ denotes tensor contraction and tr denotes the trace of a tensor. The heat flux is given by the constitutive equation

$$\mathbf{q} = -\frac{\kappa_\mathrm{c,t}}{c}\,\nabla h\,, \tag{4}$$

with the conductivity

$$\kappa_\mathrm{c,t} = \begin{cases} \kappa\,, & h < h_\mathrm{m}\,, \\ 0\,, & h \ge h_\mathrm{m}\,. \end{cases} \tag{5}$$

For cold ice ($h < h_\mathrm{m}$), this is Fourier's law of heat conduction, while for temperate ice ($h \ge h_\mathrm{m}$), the heat flux is omitted because of the vanishing temperature gradient ($\nabla T_\mathrm{m} = 0$) and the negligibly small (at least for small water content, $W \ll 1$) water diffusion.

3. Polythermal slab

To reduce the problem of a polythermal ice mass to a one-dimensional problem, we apply the plane strain approximation for a two-dimensional flow in the vertical x-z plane of a parallel-sided slab with constant and steady thickness H and constant inclination angle γ, and without dependencies on the transverse y coordinates (Fig. 2). Furthermore, we impose uniformity in the down-slope (x) direction, that is, $\partial\psi/\partial x = 0$ for any field quantity ψ. Thermomechanical coupling is omitted, thus strain heating due to horizontal shearing is prescribed (e.g., Greve, 1997; Greve and Blatter, 2009),

$$\operatorname{tr}(\mathbf{t}\cdot\mathbf{D}) = 2A\,(\rho g\sin\gamma)^4\,(H-z)^4\,. \tag{6}$$

Otherwise, the downslope velocity profile $v_x(z)$ and basal sliding are not relevant for the problem in consideration. Owing to the assumed uniformity in x-direction and the plane strain approximation, the continuity equation (mass balance) takes the form $\partial v_z/\partial z = 0$ for the slab problem, so that the velocity component in z-direction, v_z, is constant over depth, $v_z = \mathrm{const}$. Due to the kinematic boundary conditions, this means that the accumulation/ablation rate at the slab surface is equal to the melting/freezing rate at the base (and both are equal to $-v_z$).

With all these conditions, and neglect of water diffusion, the balance equation for enthalpy, Eq. (3), is reduced to

$$\frac{\partial h}{\partial t} = -v_z\frac{\partial h}{\partial z} + \frac{1}{\rho\,c}\,\frac{\partial}{\partial z}\left(\kappa_\mathrm{c,t}\,\frac{\partial h}{\partial z}\right) + \frac{2A}{\rho}\,(\rho g\sin\gamma)^4(H-z)^4\,. \tag{7}$$

We restrict this study to the Canadian-type polythermal slab. The imposed enthalpy boundary condition at the surface of the cold layer is

$$h|_{z=H} = h_\mathrm{s}(t) = c\,T_\mathrm{s}(t)\,. \tag{8}$$

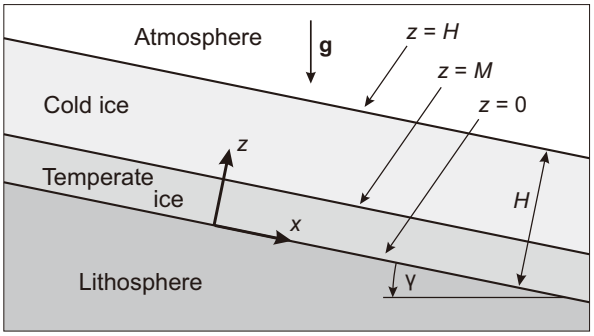

Figure 2: Polythermal parallel-sided ice slab geometry and coordinate system (adapted from Greve and Blatter, 2009).

Depending on the direction of the ice flow through the CTS, melting and freezing conditions must be distinguished. Let

$$a_{\mathrm{m}}^{\perp} = w_z - v_z \tag{9}$$

be the ice volume flux relative to the moving CTS, where $w_z = \mathrm{d}M/\mathrm{d}t$ is the kinematic (migration) velocity of the CTS in z-direction. Melting conditions are then characterised by $a_{\mathrm{m}}^{\perp} > 0$ and freezing conditions by $a_{\mathrm{m}}^{\perp} < 0$. We limit our considerations to the case that the kinematic velocity of the CTS is smaller than the ice velocity in z-direction ($|w_z| < |v_z|$), so that melting and freezing conditions correspond to downward ($v_z < 0$) and upward ice motion ($v_z > 0$), respectively.

For melting conditions, ice at the melting temperature with no liquid water flows from the cold into the temperate layer, where water is produced along a trajectory of an ice particle by strain heating, thus

$$h^+ = h^- = h_{\mathrm{m}} \quad (W^- = 0)\,, \qquad \left(\frac{\partial h}{\partial z}\right)^+ = 0 \tag{10}$$

(where the cold layer is defined as the positive, and the temperate layer as the negative side of the CTS). Together with the imposed surface enthalpy h_{s}, the enthalpy h_{m} at the CTS and the vanishing enthalpy gradient constitute three boundary conditions for the cold layer, which determine the evolution of the enthalpy profile and the thickness of the cold layer, thus also the position of the CTS. Since we have neglected water diffusion in the temperate layer, the enthalpy h_{m} at the CTS alone determines the evolution of the enthalpy profile in the temperate layer; no additional basal boundary condition is required. However, if a regularising small water diffusion were applied, an additional basal boundary condition would be needed, which then should be chosen carefully in order not to influence the numerical solution significantly (for instance, a zero-flux condition).

For freezing conditions, the enthalpy released by freezing of water flows into the cold ice along the enthalpy gradient,

$$h^+ = h_{\mathrm{m}}\,, \qquad \frac{\kappa}{\rho c}\left(\frac{\partial h}{\partial z}\right)^+ = (h^- - h_{\mathrm{m}})\, a_{\mathrm{m}}^{\perp}\,. \tag{11}$$

With $a_{\mathrm{m}}^{\perp} < 0$, $(\partial h/\partial z)^+$ can be strictly negative and $(h^- - h_{\mathrm{m}})$ strictly positive (equivalent to $W^- > 0$, discontinuous water content at the CTS). The advection equation for enthalpy in the temperate layer requires one boundary condition, for which we use the enthalpy at the ice base. Assuming a vanishing water content of the basal ice yields

$$h|_{z=0} = h_{\mathrm{m}}\,. \tag{12}$$

For the cold layer, the Dirichlet conditions (8) (prescribed surface enthalpy) and $(11)_1$ determine the evolution of the enthalpy profile, and condition $(11)_2$ can be used to determine the evolution of the CTS position by solving it for the kinematic velocity w_z that is contained in the volume flux $a_{\mathrm{m}}^{\perp}$.

Equation (7) with $\kappa_{\mathrm{t}} = 0$ for the temperate layer is equivalent to the accumulation of water produced by strain heating along trajectories. As stated above, we only consider the case $|w_z| < |v_z|$, so that melting (freezing) conditions

correspond to downward (upward) ice motion. Therefore, the water content tends to increase downwards from the CTS for melting conditions and upwards from the bed for freezing conditions.

Equations (7)–(12), to be complemented by an initial enthalpy profile h_{init}, constitute the problem of the Canadian-type polythermal parallel-sided slab. Under the additional assumption of steady-state conditions ($\partial\psi/\partial t = 0$ for any field quantity ψ), they can be solved exactly, with the exception of the position of the CTS that must be obtained with a numerical root-finding algorithm (for details see Greve (1997) or Greve and Blatter (2009)). For the general, transient case, a numerical solution is required.

4. Numerical methods

An established strategy to compute polythermal ice masses numerically is to split the computational domain into two distinct domains of cold and temperate ice, and compute the respective temperature and water content on two different grids (Blatter and Hutter, 1991; Greve, 1997; Pettersson et al., 2007). However, for the sake of simplicity, it is desirable to produce a numerical solution of the problem with a one-layer scheme, i.e., on one grid that spans the entire polythermal domain. Here, we describe possibilities for enthalpy-based two-layer and one-layer schemes for both melting and freezing conditions at the CTS.

For all schemes, time is discretized by

$$t_n = t_{\mathrm{init}} + n\Delta t \quad (n = 0 \ldots n_{\max}) \,, \tag{13}$$

where t_{init} is the initial time of the respective simulation, n is the discrete time index and Δt the time step. We have developed explicit (Euler-forward) and implicit (Euler-backward) versions of all schemes, based on second-order centred finite differences for the first and second derivatives with respect to z in the diffusion-advection equation in the cold layer (Eq. (7) with $\kappa_{\mathrm{c}} = \kappa$), and upstream first-order differences for the first derivatives in the advection equation in the temperate layer (Eq. (7) with $\kappa_{\mathrm{t}} = 0$).

4.1. Two-layer front-tracking scheme

The surface of the cold layer is at $z = H$, the bottom of the cold and top of the temperate layer (thus the CTS) at $z = M(t)$, and the bottom of the temperate layer at $z = 0$ (Fig. 2). To solve the enthalpy equation (7), we map both layers separately to layers of thickness unity,

$$\zeta_{\mathrm{c}} = \frac{z - M(t)}{H - M(t)} \,, \quad \zeta_{\mathrm{t}} = \frac{z}{M(t)} \,, \quad \tau = t \,, \tag{14}$$

where ζ_{c} and ζ_{t} are the transformed vertical coordinates in the cold and temperate layer, respectively, and τ is the transformed time. The CTS is therefore fixed with the lower and upper boundaries of the cold and temperate domains ($\zeta_{\mathrm{c}} = 0$ / $\zeta_{\mathrm{t}} = 1$), respectively. The transformed equations (7) are for the cold layer

$$\begin{aligned} \frac{\partial h}{\partial \tau} &= \frac{w_z\,(1-\zeta_{\mathrm{c}}) - v_z}{H - M} \frac{\partial h}{\partial \zeta_{\mathrm{c}}} + \frac{\kappa}{\rho\, c} \frac{1}{(H-M)^2} \frac{\partial^2 h}{\partial \zeta_{\mathrm{c}}^2} \\ &\quad + \frac{2A}{\rho} (\rho g \sin\gamma)^4 (H-M)^4 (1-\zeta_{\mathrm{c}})^4 \,, \end{aligned} \tag{15}$$

and for the temperate layer

$$\frac{\partial h}{\partial \tau} = \frac{w_z\,\zeta_{\mathrm{t}} - v_z}{M} \frac{\partial h}{\partial \zeta_{\mathrm{t}}} + \frac{2A}{\rho} (\rho g \sin\gamma)^4 (H - M\zeta_{\mathrm{t}})^4 \,, \tag{16}$$

where $w_z = \mathrm{d}M/\mathrm{d}t$ is the kinematic velocity of the CTS introduced in Section 3.

The spatial grids for the cold and temperate domain are defined by

$$(\zeta_{\mathrm{c}})_{k_{\mathrm{c}}} = \frac{k_{\mathrm{c}}}{k_{\mathrm{c,max}}} \quad (k_{\mathrm{c}} = 0 \ldots k_{\mathrm{c,max}}) \tag{17}$$

and

$$(\zeta_\mathrm{t})_{k_\mathrm{t}} = \frac{k_\mathrm{t}}{k_\mathrm{t,max}} \quad (k_\mathrm{t} = 0 \ldots k_\mathrm{t,max}) \,, \tag{18}$$

where k_c and k_t are the discrete grid indices for the two domains, and $k_\mathrm{c,max}$ and $k_\mathrm{t,max}$ denote the number of grid points in the domains. For each time step from a given time t_n to the new time $t_{n+1} = t_n + \Delta t$, Eqs. (15) and (16) are solved on these grids with the discretizations described above.

For melting conditions at the CTS, the enthalpy h_s at the surface, the enthalpy h_m and the enthalpy gradient on the cold side of the CTS are defined, thus the position of the CTS is determined by the enthalpy profile in the cold layer alone. With the two boundary conditions for the cold layer, given surface enthalpy h_s and given enthalpy h_m at the given CTS, $z = M_n$, obtained for t_n, an integration step of Eq. (15) does not generally result in a vanishing enthalpy gradient at M_n. By approximating the enthalpy profile around M_n by a quadratic parabola, the position of the vertex of the parabola is a first approximation $M_{n+1}^{(1)}$ of the CTS position at the new time t_{n+1}. The position can then be iterated (iteration index i) to the desired accuracy,

$$M_{n+1}^{(i+1)} = M_{n+1}^{(i)} - \left(\frac{\partial h}{\partial z} \right)^{+} \Bigg|_{n+1}^{(i)} \Bigg/ \left(\frac{\partial^2 h}{\partial z^2} \right)^{+} \Bigg|_{n+1}^{(i)} \,, \tag{19}$$

using the first and second derivative of the enthalpy profile at $M_{n+1}^{(i)}$. Furthermore, from the displacement of the CTS, we obtain the kinematic velocity $(w_z)_{n+1}$ of the CTS via

$$(w_z)_{n+1} = \frac{M_{n+1} - M_n}{\Delta t} \,. \tag{20}$$

For freezing conditions, the transition condition at the CTS (Eq. $(11)_2$) in the transformed cold layer yields an equation for the ice volume flux $a_\mathrm{m}^\perp$ through the CTS,

$$a_\mathrm{m}^\perp = \frac{\kappa}{(h^- - h_m)\, \rho c \, (H - M)} \left(\frac{\partial h}{\partial \zeta} \right)^{+} . \tag{21}$$

The discretized version of this equation provides the volume flux $(a_\mathrm{m}^\perp)_{n+1}$ and, via Eq. (9), the kinematic velocity of the CTS,

$$(w_z)_{n+1} = (a_\mathrm{m}^\perp)_{n+1} + v_z \,, \tag{22}$$

which allows to update the CTS position,

$$M_{n+1} = M_n + (w_z)_{n+1} \Delta t \,. \tag{23}$$

4.2. Conventional one-layer scheme

In contrast to the two-layer scheme discussed in Section 4.1, in the conventional one-layer scheme, which corresponds to the enthalpy scheme by Aschwanden et al. (2012), Eq. (7) is solved for the entire polythermal slab on one grid in the z-domain. It is defined by

$$z_k = k \Delta z = H \frac{k}{k_\mathrm{max}} \quad (k = 0 \ldots k_\mathrm{max}) \,, \tag{24}$$

where k is the discrete grid index, Δz the grid spacing (resolution), and k_max denotes the number of grid points. This grid is also used for the modified one-layer schemes described below (Sections 4.3, 4.4).

The CTS must be tracked on this grid. The cold and temperate layers can be discriminated by the contour $h = h_\mathrm{m}$, and we define the CTS position, $k = k_\mathrm{cts}$, as the uppermost grid point of the temperate part (that is, the uppermost grid point for which $h \geq h_\mathrm{m}$ holds).

Transition conditions at the CTS are not accounted for explicitly. In our one-dimensional implementation, for a melting CTS, where the ice flows downwards, the surface boundary condition (given enthalpy) and the assumed continuity of the enthalpy field at the CTS define the entire enthalpy profile $h_{k,n+1}$ at the new time t_{n+1} when the profile $h_{k,n}$ at the old time t_n is known. Boundary conditions at the base are not necessary because of the advection equation

in the temperate layer. Therefore, only one boundary condition at the surface of the cold layer is required to obtain a unique solution.

Although the conductivity is constant in the cold and temperate layers ($\kappa_c = \kappa$ and $\kappa_t = 0$, respectively; Eq. (5)), the discretization of the diffusion term in Eq. (7) must take into account the variation of the conductivity at least across the CTS, i.e., for $k = k_{cts}$:

$$\begin{aligned} \frac{\partial}{\partial z}\left(\kappa_{c,t}\,\frac{\partial h}{\partial z}\right) &\sim \frac{(\kappa_{c,t}\,\frac{\partial h}{\partial z})_{k+1/2,n} - (\kappa_{c,t}\,\frac{\partial h}{\partial z})_{k-1/2,n}}{\Delta z} \\ &\sim \frac{\kappa_c(h_{k+1,n} - h_{k,n}) - \kappa_t(h_{k,n} - h_{k-1,n})}{\Delta z^2} \end{aligned} \tag{25}$$

(T. Kleiner, personal communication, February 2014; Kleiner et al., 2015). Omission of this, and discretizing the diffusion term in the form $\kappa_{c,t}\,(\partial^2 h/\partial z^2)$ instead, results in a faulty enthalpy profile that violates the melting-CTS transition condition $(10)_2$ (zero enthalpy gradient at the cold side of the CTS).

For freezing conditions, the method must fail because it is not consistent with the discontinuity of the enthalpy field at the CTS that results from the discontinuity of the water content (Eq. (11) and following text).

4.3. One-layer melting CTS scheme

We propose an alternative one-layer scheme for melting conditions that enforces explicitly the zero enthalpy gradient at the cold side of the CTS (Eq. $(10)_2$). For this scheme, the discretization of the diffusion term in Eq. (7) need not consider a conductivity that depends on the position z like in Eq. (25); instead, it can be done in the form

$$\begin{gathered} \kappa_{c,t}\,\frac{\partial^2 h}{\partial z^2} \sim (\kappa_{c,t})_{k,n}\,\frac{h_{k+1,n} - 2h_{k,n} + h_{k-1,n}}{\Delta z^2}\,, \\ \text{with } (\kappa_{c,t})_{k,n} = \begin{cases} \kappa_t\,, & k = 0 \ldots k_{cts}\,, \\ \kappa_c\,, & k = k_{cts}+1 \ldots k_{max}\,. \end{cases} \end{gathered} \tag{26}$$

Each time step is now divided into two iteration steps. The predictor step for solving the enthalpy equation (7) is carried out for the entire polythermal slab as in the conventional one-layer scheme (Section 4.2). This provides a preliminarily updated enthalpy profile $h^{(1)}_{k,n+1}$. For this profile, the updated position of the CTS ($k = k_{cts}$, uppermost temperate grid point) and the updated conductivities $\kappa_{c,t}$ (according to Eq. (5)) for each grid point are determined.

The corrector step affects only the cold layer. We repeat the forward step for the enthalpy equation from the grid point $k = k_{cts}$ to the surface ($k = k_{max}$), discretizing the zero enthalpy gradient on the cold side of the CTS (Eq. $(10)_2$) by

$$h_{k_{cts},n+1} = h_{k_{cts}+1,n+1}\,. \tag{27}$$

This provides an enthalpy profile $h^{(2)}_{k,n+1}$ for the cold layer only. The complete, updated enthalpy profile $h_{k,n+1}$ is assembled by the predictor step for the temperate layer and the corrector step for the cold layer,

$$h_{k,n+1} = \begin{cases} h^{(1)}_{k,n+1}\,, & k = 0 \ldots k_{cts}\,, \\ h^{(2)}_{k,n+1}\,, & k = k_{cts}+1 \ldots k_{max}\,. \end{cases} \tag{28}$$

4.4. One-layer freezing CTS scheme

Owing to the discontinuous enthalpy and enthalpy gradient at the CTS (Eq. (11)), a one-layer scheme for freezing conditions at the CTS is more difficult to implement. The advection equation in the temperate layer (Eq. (7) with $\kappa_t = 0$) only requires one boundary condition, which is the Dirichlet condition (12) (imposed value of the basal enthalpy corresponding to zero water content). The advection equation can therefore be solved independently of the cold layer. For each time step (from t_n to t_{n+1}), we do so for the entire polythermal slab, which provides a first profile $h^{(1)}_{k,n+1}$ that is only valid for the temperate layer from the ice base to the yet unknown new position of the CTS.

We then solve the diffusion-advection equation (Eq. (7) with $\kappa_c = \kappa$) in the cold layer. Based on the CTS position M_n at time t_n (in contrast to the one-layer melting CTS scheme, the CTS is tracked with sub-grid precision, as will be explained below), we denote the uppermost grid point in the temperate layer as k_{cts}, and compute the enthalpy profile from the grid point $k = k_{\mathrm{cts}}$ to the surface ($k = k_{\max}$). A quadratic extrapolation using the three grid points above k_{cts} is used as a boundary condition:

$$h_{k_{\mathrm{cts}},n+1} = 3\,h_{k_{\mathrm{cts}}+1,n+1} - 3\,h_{k_{\mathrm{cts}}+2,n+1} + h_{k_{\mathrm{cts}}+3,n+1}\,. \tag{29}$$

This step provides a second enthalpy profile $h^{(2)}_{k,n+1}$ that is valid for the cold layer from the CTS to the surface.

Tracking of the CTS is carried out by using the transition condition $(11)_2$. For this purpose, the enthalpy on the temperate side of the CTS is interpolated by

$$h^{-}_{n+1} \sim h^{(1)}_{k_{\mathrm{cts}}} + \frac{M_n - (z_{k_{\mathrm{cts}}})_n}{\Delta z}\left(h^{(1)}_{k_{\mathrm{cts}}+1,n+1} - h^{(1)}_{k_{\mathrm{cts}},n+1}\right), \tag{30}$$

and the enthalpy gradient on the cold side of the CTS is discretized by

$$\left(\frac{\partial h}{\partial z}\right)^{+}_{n+1} \sim \frac{h^{(2)}_{k_{\mathrm{cts}}+1,n+1} - h^{(2)}_{k_{\mathrm{cts}},n+1}}{\Delta z}\,. \tag{31}$$

Inserting Eqs. (30) and (31) in Eq. $(11)_2$ yields the updated volume flux $(a^{\perp}_{\mathrm{m}})_{n+1}$. According to Eqs. (22) and (23), this allows to update subsequently the kinematic velocity of the CTS, $(w_z)_{n+1}$, and the CTS position, M_{n+1}. The latter actually constitutes a sub-grid tracking of the CTS that goes beyond the grid-limited precision provided by k_{cts} (uppermost temperate grid point).

The final, updated enthalpy profile $h_{k,n+1}$ is assembled from $h^{(1)}_{k,n+1}$ and $h^{(2)}_{k,n+1}$ according to Eq. (28).

5. Set-up of the numerical experiments

For all numerical experiments presented in this work, the thickness of the polythermal slab is $H = 200\,\mathrm{m}$ and the inclination angle $\gamma = 4^\circ$ (Fig. 2). For melting conditions at the CTS, we set $v_z = -0.2\,\mathrm{m\,a^{-1}}$, and for freezing conditions $v_z = +0.2\,\mathrm{m\,a^{-1}}$. All experiments are designed such that the condition $|w_z| < |v_z|$ (see Eq. (9) and the following text) is fulfilled at all times.

Steady states for enthalpy profiles, or, equivalently, for temperature and water-content profiles, are computed for melting conditions with surface temperatures of -1°C and -3°C, and for freezing conditions with -6°C and -10°C.

Transient experiments are carried out for melting conditions with step changes of the surface temperature from -4°C to -2°C and vice versa, and for freezing conditions with step changes from -10°C to -6°C and vice versa. The step changes are employed at the initial time $t_{\mathrm{init}} = 0$, and the initial conditions for these four scenarios are steady states for the respective initial temperatures.

Furthermore, we perform experiments with sinusoidal variations of the surface temperature with a mean value of -2°C and an amplitude of 1 K for a melting CTS, and a mean value of -8°C and an amplitude of 2 K for a freezing CTS. The initial conditions for these scenarios are steady states for the mean surface temperatures (-2°C and -8°C, respectively), and two different periods of 100 and 500 years are employed for both cases.

All discussed experiments with the two-layer front-tracking scheme are run with a resolution of 100 grid points in each layer and a time step of 0.01 years. The standard resolution and time step for experiments with the three different one-layer schemes are 1 m (that is, 200 grid points) and 0.01 years, respectively. However, we also use the combinations 2 m (100 grid points) / 0.01 years and 0.5 m (400 grid points) / 0.002 years; this is indicated in the captions of the corresponding figures. All of these combinations are stable for both the explicit and implicit versions of the several numerical schemes. The implicit schemes allow for larger time steps of up to 100 years; however, then the accuracy of transient solutions is affected. As long as small time steps (within the range of stability of the explicit schemes) are used, differences of results between the explicit and implicit schemes are very small and virtually indistinguishable in normal plots. Therefore, we only show results computed with the explicit schemes.

6. Results

6.1. Two-layer front-tracking scheme

The steady-state results of the two-layer front-tracking tracking scheme can be verified with the exact, analytical solutions (Greve, 1997; Greve and Blatter, 2009). Figure 3 shows the computed steady-state solutions (enthalpy profiles converted back to temperature and water-content profiles) for both a melting and freezing CTS and prescribed constant surface enthalpies $h_s = c\,T_s$ corresponding to the surface temperatures listed in Section 5. These steady states agree to high accuracy with the exact solutions (not shown explicitly). The positions of the CTS coincide within about 0.3 m, which is better than the grid resolution. In particular, according to its design, the scheme handles the discontinuities for freezing conditions at the CTS well.

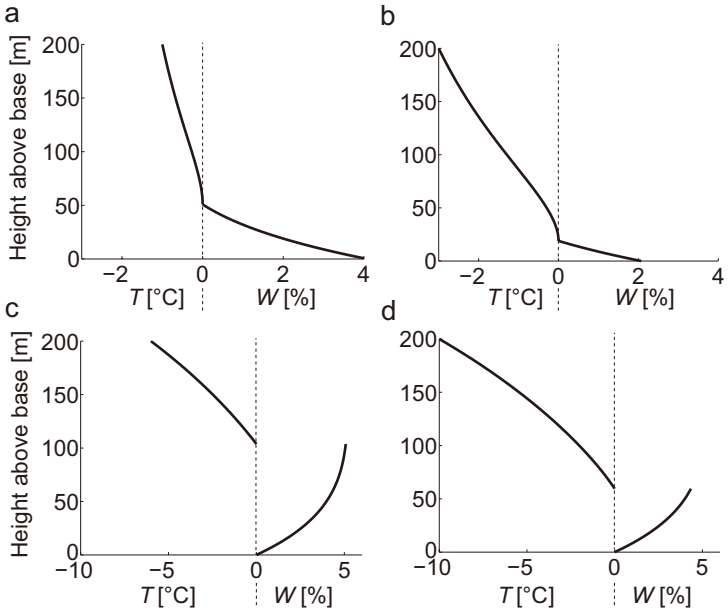

Figure 3: Steady-state profiles of temperature T (in the cold layer, values ≤ 0) and water content W (in the temperate layer, values ≥ 0) of the parallel-sided slab with a melting CTS ($v_z = -0.2\,\mathrm{m\,a^{-1}}$), computed with the two-layer front-tracking scheme. (a) surface temperature $T_s = -1°\mathrm{C}$, (b) $T_s = -3°\mathrm{C}$. Same for a freezing CTS ($v_z = +0.2\,\mathrm{m\,a^{-1}}$) with (c) surface temperature $T_s = -6°\mathrm{C}$, (d) $T_s = -10°\mathrm{C}$.

We also calculated the various transient scenarios (step changes in the surface boundary conditions, sinusoidally varying surface conditions; see Section 5) with the two-layer front-tracking tracking scheme. The results (CTS positions and maximum water contents as functions of time for the step changes, CTS positions only for the sinusoidal forcings) are shown below in Figs. 5-8 and will be used as references to test the performance of the one-layer schemes.

All runs were performed with both the explicit and the implicit version of the two-layer front-tracking tracking scheme. The steady-state solutions are almost independent of the time step (within stability limits). For the transient scenarios, time steps longer than the standard time step (Section 5) act like a low-pass filter (again, within stability limits). They have little influence on the results as long as the time step is smaller than the rate of change of the conditions. Otherwise, delayed responses and dampenings occur, which, for the sinusoidal forcings, results in reduced amplitudes and phase shifts of the oscillating solutions.

6.2. Conventional one-layer scheme

Figure 4 (black line) shows the steady-state solution (enthalpy profile converted back to temperature and water-content profiles) for a melting CTS and a surface enthalpy corresponding to $T_s = -3°\mathrm{C}$ computed with the conventional one-layer scheme, which corresponds to the enthalpy scheme by Aschwanden et al. (2012). The solution is almost identical to the exact solution and the one computed with the two-layer front-tracking scheme (Fig. 3b).

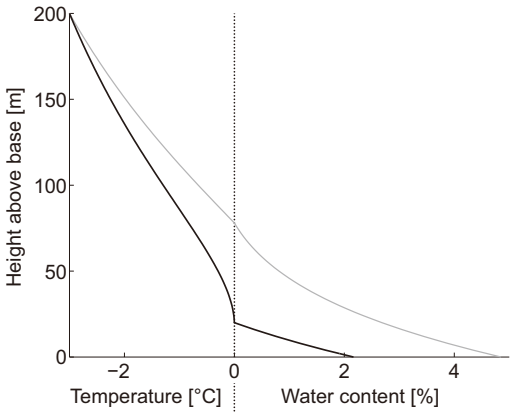

Figure 4: Black, lower line: Steady-state profiles of temperature (in the cold layer, values ≤ 0) and water content (in the temperate layer, values ≥ 0) corresponding to the steady-state solution shown in Fig. 3b for a melting CTS ($v_z = -0.2\,\mathrm{m\,a^{-1}}$), computed with the conventional one-layer scheme. Grey, upper line: Same, but the jump of the conductivity at the CTS was disregarded in the discretization of the diffusion term in Eq. (7).

However, this result is only obtained if the jump of the conductivity at the CTS is properly accounted for in the discretization of the diffusion term in the enthalpy equation (Eq. (25)). Otherwise (discontinuity of the conductivity at the CTS disregarded, discretization like in Eq. (26)), a greatly flawed solution results (grey line in Fig. 4). This solution has significantly larger enthalpies along the entire profile except for the surface, the CTS position is ~ 4 times higher above the base than in the correct solution, and it does not meet the required transition condition $(10)_2$ at the CTS.

6.3. One-layer melting CTS scheme

Figure 5 shows a comparison of the one-layer melting CTS scheme with the two-layer front-tracking scheme that is considered to provide reference solutions. It shows the position of the CTS and the basal water content for the step-change scenarios from $T_s = -4°\mathrm{C}$ to $-2°\mathrm{C}$ and vice versa (Section 5). For the one-layer scheme, the three different resolutions of 0.5 m, 1 m (standard) and 2 m have been employed.

The transitions between the two states show some asymmetric behaviour, depending on whether the CTS moves in the direction of the cold or the temperate layer. The evolution of the CTS position is smooth for the two-layer scheme, whereas it occurs in steps for the one-layer scheme. This is a consequence of the CTS tracking on the discrete grid in the one-layer scheme (Section 4.3), which only allows an accuracy of one grid spacing. The results obtained with the one-layer scheme (CTS position, basal water content) show good convergence with increasing resolution to the reference solution obtained with the two-layer scheme.

The computed CTS positions for the two scenarios with sinusoidal forcings (Section 5) are shown in Fig. 6. Again, the results obtained with the two-layer scheme are very smooth, while the one-layer scheme produces step changes of the CTS position that reflect the resolution. This becomes particularly evident for the short period (100 years), for which the amplitude of the variability of the CTS position is less then 2 m. It can only be reproduced reasonably well by the highest resolution of 0.5 m, while the 1-m resolution reproduces the variability only rudimentarily, and the 2-m resolution yields only an average CTS position. For the long period (500 years), the results are less susceptible to the grid resolution, of comparable quality to those for the step-change forcing shown in Fig. 5a, and the highest 0.5-m resolution matches closely the solution for the two-layer front-tracking method.

6.4. One-layer freezing CTS scheme

We now compare the performance of the one-layer freezing CTS scheme with that of the two-layer front-tracking scheme. Figure 7 shows the evolution of the height of the CTS above the bed and the water content at the temperate side of the CTS for the step-change scenarios from $T_s = -10°\mathrm{C}$ to $-6°\mathrm{C}$ and vice versa (Section 5). Like in Section 6.3, for the one-layer scheme, the three different resolutions of 0.5 m, 1 m (standard) and 2 m have been employed.

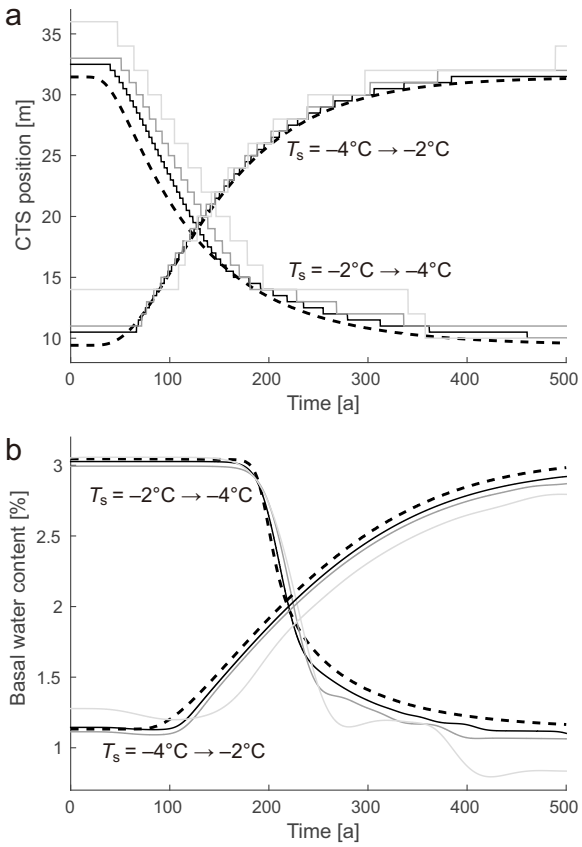

Figure 5: Comparison between the one-layer melting CTS scheme (solid lines) and the two-layer front-tracking scheme (dashed lines) for melting conditions ($v_z = -0.2\,\mathrm{m\,a^{-1}}$). (a) Position of the CTS and (b) basal water content for a step change of the surface temperature from $T_s = -4°\mathrm{C}$ to $-2°\mathrm{C}$ (rising curves) and vice versa (falling curves) at time $t = 0$. The three different solid lines correspond to grid resolutions of 0.5 m (black), 1 m (medium-grey) and 2 m (light-grey).

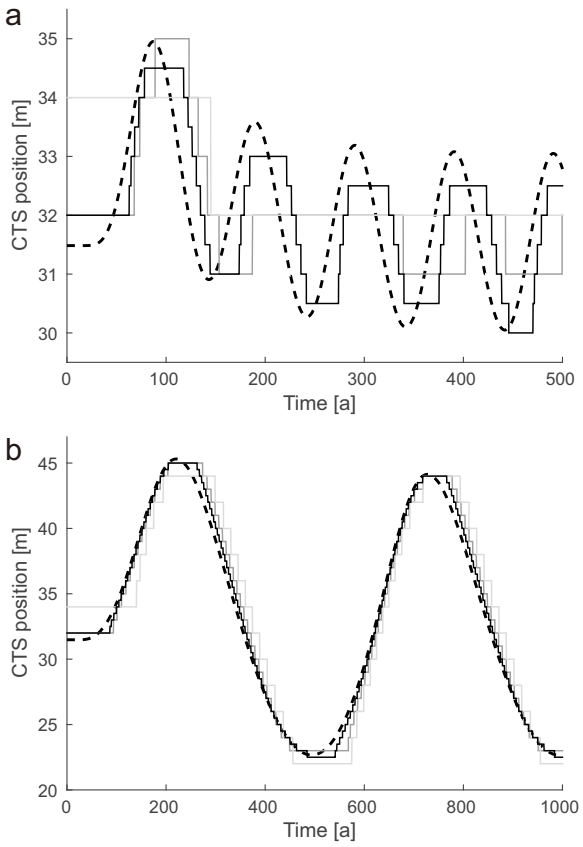

Figure 6: Comparison between the one-layer melting CTS scheme (solid lines) and the two-layer front-tracking scheme (dashed lines) for melting conditions ($v_z = -0.2\,\mathrm{m\,a^{-1}}$). (a) Position of the CTS for a sinusoidal oscillation of the surface temperature centred at $T_\mathrm{s} = -2^\circ\mathrm{C}$ with an amplitude of 1 K and a period of 100 years. (b) same as (a), but with a period of 500 years. The three different solid lines correspond to grid resolutions of 0.5 m (black), 1 m (medium-grey) and 2 m (light-grey).

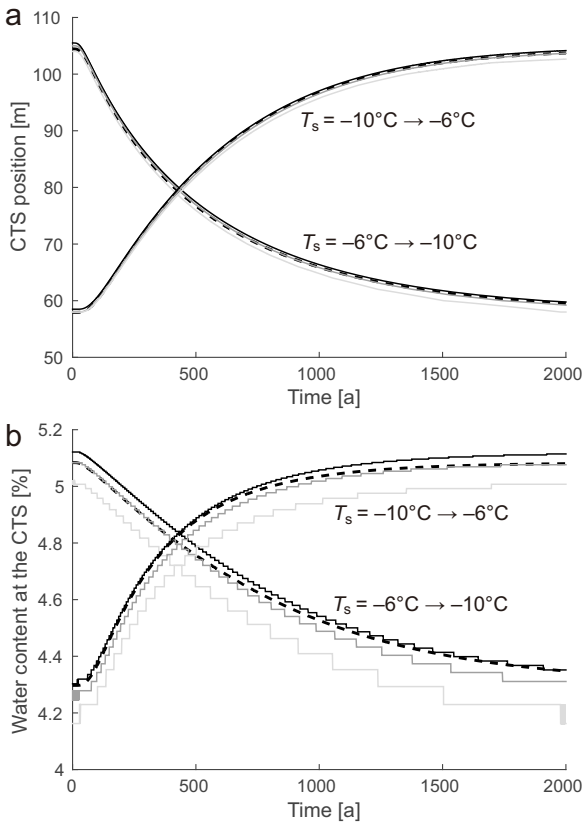

Figure 7: Comparison between the one-layer freezing CTS scheme (solid lines) and the two-layer front-tracking scheme (dashed lines) for freezing conditions ($v_z = +0.2\,\mathrm{m\,a^{-1}}$). (a) Position of the CTS and (b) water content at the temperate side of the CTS for a step change of the surface temperature from $T_s = -10°\mathrm{C}$ to $-6°\mathrm{C}$ (rising curves) and vice versa (falling curves) at time $t = 0$. The three different solid lines correspond to grid resolutions of 0.5 m (black), 1 m (medium-grey) and 2 m (light-grey).

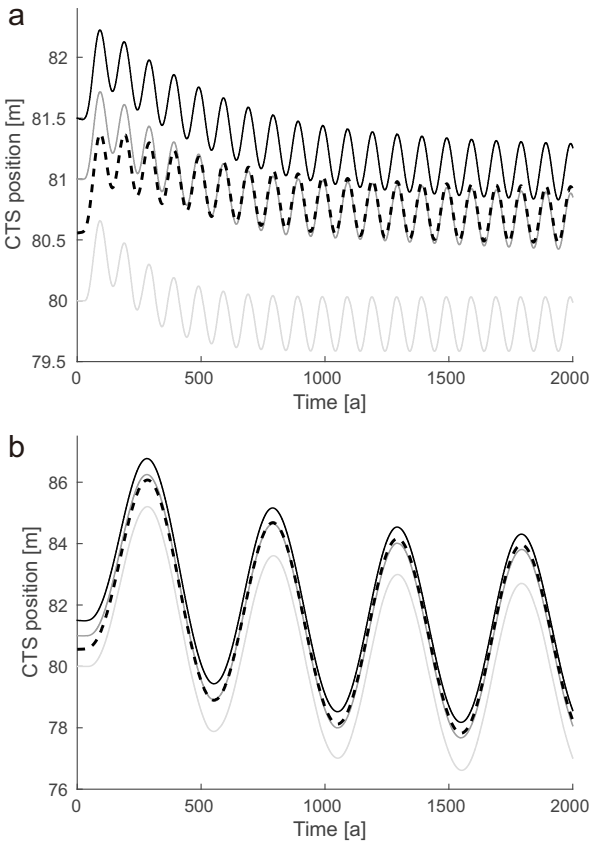

Figure 8: Comparison between the one-layer freezing CTS scheme (solid lines) and the two-layer front-tracking scheme (dashed lines) for freezing conditions ($v_z = +0.2\,\mathrm{m\,a^{-1}}$). (a) Position of the CTS for a sinusoidal oscillation of the surface temperature centred at $T_\mathrm{s} = -8^\circ\mathrm{C}$ with an amplitude of 2 K and a period of 100 years. (b) same as (a), but with a period of 500 years. The three different solid lines correspond to grid resolutions of 0.5 m (black), 1 m (medium-grey) and 2 m (light-grey).

Since the upward-moving ice reduces the response of the system to surface perturbations at a given depth, the freezing CTS requires a longer time for adjustment than the melting CTS (compare with Fig. 5a). A further, notable difference is that the CTS evolution is smooth for both the one-layer and two-layer schemes. This is a consequence of the sub-grid tracking of the CTS employed in the one-layer freezing CTS scheme (Section 4.4), whereas the one-layer melting CTS scheme allows tracking the CTS only with grid-limited precision (Section 4.3). By contrast, the computed water content at the CTS shows some step changes for the one-layer scheme, while it is also smooth for the two-layer scheme. For all three resolutions of the one-layer scheme, the results agree well with those of the two-layer scheme; the largest (but still acceptable) discrepancy is found for the water content at the CTS computed with the 2-m resolution.

Figure 8 shows the evolutions of the CTS positions for the two scenarios with sinusoidal forcings (Section 5), computed with the one-layer freezing CTS scheme and the two-layer scheme. The amplitude of the variations of the CTS position is substantially smaller than that of the melting CTS even though the amplitude of the surface perturbation is larger (2 K vs. 1 K), which is again due to the upward direction of the ice motion that delays and dampens changes of the surface conditions at depth. For both periods (100 and 500 years) and all resolutions, the agreement to the reference results (two-layer scheme) is within about the grid resolution of the one-layer scheme. As already observed in Fig. 7a, the sub-grid tracking leads to a smooth evolution of the CTS, and the simulated amplitudes agree very well for all schemes and resolutions.

7. Discussion and conclusion

The conventional one-layer scheme, which corresponds to the implementation of the enthalpy method by Aschwanden et al. (2012), does not explicitly take into account the Stefan-type energy- and mass-flux matching conditions at the CTS that are crucial for determining the position of the CTS. Nevertheless, we have demonstrated that this scheme can determine the CTS position for the case of melting conditions correctly. However, this depends critically on the proper numerical handling of the discontinuity of the conductivity across the CTS and is therefore prone to failure if the implementation is not done with great care. For the case of freezing conditions with the associated discontinuity of the enthalpy at the CTS, the conventional one-layer scheme fails inevitably.

Two-layer front-tracking schemes, using a time-dependent terrain-following coordinate transformation for the cold and temperate layers separately (Blatter and Hutter, 1991; Greve, 1997; Pettersson et al., 2007), can also be used in conjunction with the enthalpy method. We have constructed such a scheme, and have shown that it produces very good results for both melting and freezing conditions. However, schemes using only one grid for the entire polythermal slab are simpler to implement in existing ice sheet models and therefore more desirable.

Therefore, we have proposed one-layer methods that modify the original enthalpy scheme by Aschwanden et al. (2012) in order to treat explicitly the transition conditions at the CTS for both cases of a melting and freezing CTS. The proposed methods work well in our one-dimensional model, provided that the time steps and grid resolutions are sufficiently small. We expect them to work as well in shallow ice sheet models, where the thermodynamics neglects horizontal diffusive heat fluxes and thus treats vertical enthalpy or temperature profiles essentially in a one-dimensional way. Horizontal advective heat fluxes can be treated as additional source terms of the vertical profiles. In fact, we have already implemented the one-layer melting CTS scheme in the ice sheet model SICOPOLIS (e.g., Sato and Greve, 2012; Greve and Herzfeld, 2013; URL http://www.sicopolis.net/), which, despite the required adjustments for the additional physics (pressure dependence of the melting point as well as temperature-dependent heat conductivity and specific heat capacity accounted for), could be done in a fairly straightforward way (paper in preparation). With some additional effort due to the complicating horizontal diffusive heat fluxes, implementations in non-shallow (higher-order or full Stokes) ice sheet and glacier models should also be feasible.

Acknowledgements

We thank F. Saito, A. Aschwanden, E. Bueler and T. Kleiner for helpful discussions. Comments by two anonymous reviewers and the scientific editor, T. Kameda, helped to improve the manuscript. H.B. was supported by an Invitation Fellowship for Research in Japan (No. L13525) of the Japan Society for the Promotion of Science (JSPS). R.G. was supported by a JSPS Grant-in-Aid for Scientific Research A (No. 22244058).

References

Aschwanden, A., Blatter, H., 2005. Meltwater production due to strain heating in Storglaciären, Sweden. J. Geophys. Res. 110 (F4), F04024.

Aschwanden, A., Bueler, E., Khroulev, C., Blatter, H., 2012. An enthalpy formulation for glaciers and ice sheets. J. Glaciol 58 (209), 441–457.

Blatter, H., Hutter, K., 1991. Polythermal conditions in Artic glaciers. J. Glaciol. 37 (126), 261–269.

Dash, J. G., Rempel, A. W., Wettlaufer, J. S., 2006. The physics of premelted ice and its geophysical consequences. Rev. Mod. Phys. 78 (3), 695–741.

Duval, P., 1977. The role of water content on the creep of polycrystalline ice. In: Isotopes and Impurities in Snow and Ice – Proceedings of the Grenoble Symposium, August-September 1975. IAHS Publication No. 118. International Association of Hydrological Sciences, Wallingford, UK, pp. 29–33.

Fowler, A. C., 1984. On the transport of moisture in polythermal glaciers. Geophys. Astrophys. Fluid Dyn. 28 (2), 99–140.

Fowler, A. C., Larson, D. A., 1978. Flow of polythermal glaciers: 1. Model and preliminary analysis. Proc. R. Soc. Lond. A 363 (1713), 217–242.

Greve, R., 1997. A continuum-mechanical formulation for shallow polythermal ice sheets. Phil. Trans. R. Soc. Lond. A 355 (1726), 921–974.

Greve, R., Blatter, H., 2009. Dynamics of Ice Sheets and Glaciers. Springer, Berlin, Germany, etc.

Greve, R., Herzfeld, U. C., 2013. Resolution of ice streams and outlet glaciers in large-scale simulations of the Greenland ice sheet. Ann. Glaciol. 54 (63), 209–220.

Hutter, K., 1982. A mathematical model of polythermal glaciers and ice sheets. Geophys. Astrophys. Fluid Dyn. 21 (3-4), 201–224.

Hutter, K., 1993. Thermo-mechanically coupled ice-sheet response – cold, polythermal, temperate. J. Glaciol. 39 (131), 65–86.

Kleiner, T., Rückamp, M., Bondzio, J., Humbert, A., 2015. Enthalpy benchmark experiments for numerical ice sheet models. The Cryosphere 9 (1), 217–228.

Pettersson, R., Jansson, P., Huwald, H., Blatter, H., 2007. Spatial pattern and stability of the cold surface layer of Storglaciären, Sweden. J. Glaciol. 53 (180), 99–109.

Sato, T., Greve, R., 2012. Sensitivity experiments for the Antarctic ice sheet with varied sub-ice-shelf melting rates. Ann. Glaciol. 53 (60), 221–228.